Q. J. R. Meteorol. Soc. (2004), **130**, pp. 51–78 doi: 10.1256/qj.03.41

Physically based two-moment bulkwater parametrization for warm-cloud microphysics

By JEN-PING CHEN* and SEN-TSONG LIU
Department of Atmospheric Sciences, National Taiwan University, Taipei, Taiwan

(Received 6 March 2003; revised 4 June 2003)

SUMMARY

A two-moment bulkwater parametrization scheme for warm-cloud microphysics is developed via statistical analyses of results from a detailed parcel model. This computationally efficient scheme is quite accurate and produces bulkwater properties which resemble the results from a fully explicit microphysical model. It responds sensitively to the effect of aerosol types on the cloud drop number concentration and the timing of rain initiation. Diagnostic formulae are also provided for the group fall velocity, number and mass sedimentation fluxes, the radar reflectivity factor, and the effective radii of cloud drops and raindrops. This physically sound and easy to use parametrization scheme could be useful in improving the microphysical representation in regional- and cloud-scale models.

KEYWORDS: Effective radius Explicit microphysics Radar reflectivity

1. INTRODUCTION

Traditional bulkwater parametrization schemes divide the water substance in the clouds into water vapour, cloud drops, raindrops, and a few bulk categories for the ice-phase particles to simplify the computation of cloud microphysics. The conversion rates between these bulkwater categories are derived either empirically or theoretically and represented in simple forms. Such a parametrization scheme was first introduced by Kessler (1967, 1969), thus it is called the Kessler-type scheme, and has been widely applied in mesoscale cloud models (e.g. Wisner *et al.* 1972; Tripoli and Cotton 1980; Lin *et al.* 1983; Mölders *et al.* 1994) because of its high computational efficiency. However, due to a few inherent drawbacks, the Kessler-type bulkwater scheme inevitably has critical limitations. First of all, fixed forms of particle size distribution must be assumed in order to derive the conversion rates theoretically; yet, in reality, the size distribution may deviate significantly from the assumed functional forms either in time or in space (Silverman and Glass 1973; Joss and Gori 1978; Willis 1984; Zawadzki *et al.* 1994). Some studies even suggested that the commonly used Marshall–Palmer distribution is merely a statistical average of many 'instantaneous' size distributions that are actually not in the exponential forms (Joss and Gori 1978; Liu 1993). Hence the specification of particular functional forms necessarily puts artificial constraints on the conversion rates. Furthermore, for a growth equation with complicated growth kernel, an analytical solution often does not exist even if one assumes a simple form of size distribution. For instance, the collision-coalescence efficiency is strongly dependent on the particle size and aerodynamic properties of air, yet it is often set to a constant value or even unity in many bulkwater schemes (e.g. Wisner *et al.* 1972; Manton and Cotton 1977; Tripoli and Cotton 1980; Mölders *et al.* 1994). The collision-break-up kernel is even more complicated (cf. Low and List 1982b), such that getting an analytical solution mathematically for the growth equation is simply impossible.

Another important limitation in these bulkwater schemes stems from their disregard of the particle number concentration, without which many important prognostic and diagnostic properties cannot be obtained. For instance, even if an analytical solution

* Corresponding author: Department of Atmospheric Sciences, National Taiwan University, Taipei, Taiwan.
e-mail: jpchen@webmail.as.ntu.edu.tw

to the collision growth equation does exist, it might still be necessary to set the collision-coalescence efficiency to a constant value due to the unavailability of the required information on particle sizes. By including the number concentration, at least some first order size information (e.g. mean volume radius) can be derived. Moreover, the traditional Kessler scheme carries only one parameter (moment) while the assumed size distribution normally requires two or more to describe it. With only one degree of freedom, more constraints (such as fixing the slope or intercept of the Marshall–Palmer distribution (Marshall and Palmer 1948)) must be imposed to solve the growth equations, which inevitably leads to large errors. Unfortunately, different processes tend to modify different parameters of the size distribution (Srivastava 1978; Tripoli and Cotton 1980), so there is no obvious choice of the parameter to be fixed. Thus, many multi-moment schemes have been developed to overcome the deficiencies of the single-moment methods, such as the two-moment schemes of Manton and Cotton (1977), Ferrier (1994), and Carrió and Nicolini (2002), and the three-moment schemes of Clark (1974) and Clark and Hall (1983).

Another shortcoming of models neglecting number concentration is their inability to describe the influence of aerosol on clouds. Explicit microphysical models that consider only the mass concentration cannot even resolve the basic differences between maritime and continental cloud and precipitation processes, not to mention the effect of local anthropogenic emissions. Twomey (1974) proposed that anthropogenic aerosols may influence the reflectance of clouds through the modification of cloud drop number concentration. The inability to resolve such aerosol–cloud interaction is an important factor contributing to the high uncertainties in the calculations of climate forcing in regional and global modelling studies (IPCC 2001).

In this study we develop a new bulk parametrization scheme for warm-cloud microphysics following the physical–statistical approach of Lee (1989, 1992) who derived the parametrizations from the results of a detailed microphysical parcel model. This method groups the results (mixing ratios and conversion rates) of a detailed (multi-category, or multi-bin) cloud microphysical model into a smaller number of categories in a way similar to that of the traditional bulkwater schemes. The formulae of bulk conversion rates are obtained by a regression analysis of the detailed model results, which are then expressed in terms of the moments of the bulk species. In this approach no assumptions about the drop size distribution are necessary, and the growth formulae can be integrated without any simplifications of the growth kernels as is necessary in traditional bulkwater schemes. Such a parametrization scheme is physically based, with accuracy approaching the detailed models, and yet comparable in computation efficiency to the traditional bulkwater schemes. However, whereas Lee (1989) provided parametrizations of only one moment of the bulk categories—the water mass mixing ratio, here we build a set of parametrization schemes that consider not only the mass mixing ratio but also the number concentration of cloud drops and raindrops using a very detailed cloud microphysical model of Chen and Lamb (1994, 1999).

A list of symbols used is given in the appendix.

2. Method

(*a*) *Converting binned categories into bulk parameters*

Developing a parametrization scheme following Lee's (1989) physical–statistical approach requires a large dataset generated from a sophisticated microphysical model. Since the accuracy of the parametrization scheme is limited by the preciseness of the dataset, it is essential to use a microphysical model that can realistically simulate the

evolution of cloud particle size spectra under a broad range of conditions. Here we applied the multi-component model of Chen and Lamb (1994), which has demonstrated the capability of treating warm- and cold-cloud microphysics in great detail (Chen *et al.* 1997; Chen and Lamb 1999). In this model, cloud particles are classified into many bins according to both their water masses and solute masses. Here we describe the drop spectrum with 45 bins in the water component, with the largest bin limit corresponding to the mass of a spherical drop of 4.5 mm radius, and then for each successive bin with the mass reduced by one half. For the solute component we apply a high density of 90 bins, with the largest solute bin corresponding to a dry radius of 30 μm, and the subsequent bin limits reduced by a factor of 1.35 in solute mass. Note that there exists a cut-off solute mass for the activation of aerosol into cloud drops, and this cut-off seldom lies exactly at the bin limits. Yet, in most bin models particles in the same bin cannot be divided into subgroups to allow partial activation. So a fine bin resolution, such as that applied here, is desirable in order to reduce the inaccuracy associated with the discrete nature of the bin structure (cf. Kreidenwise *et al.* 2003). A method-of-moments type scheme is used to ensure number and mass conservation, as well as to minimize numerical diffusion, in calculating the evolution of the drop spectrum.

Similar to the traditional bulkwater schemes, we regroup aqueous-phase cloud particles in the detailed model into two bulk categories—cloud drops and raindrops, using 50 μm radius as the separation criterion. Note that in Chen and Lamb's original model all particles, whether activated (cloud and rain) or not (haze or interstitial aerosol particles), are treated in the same single framework. As a result, the distinction between cloud drops and interstitial aerosol particles is not so straightforward. Theoretically, one should be able to use the critical radius of the Köhler curves to determine if cloud condensation nuclei (CCN) are activated into cloud drops. However, some of the largest CCN may never reach their critical radii and remain as 'giant haze drops', and yet they are generally the largest drops during the early stage of cloud formation and act as rain embryos (Chen and Lamb 1999). So, we have relaxed the criterion for cloud drops to be of radii greater than either 2.5 μm or their critical radii. Furthermore, some of the largest CCN are activated directly into raindrops. Therefore, in our scheme a small quantity of raindrops (which we called the rain embryos) are allowed to form immediately after the air parcel is saturated (see subsections 3(e) and 4(a)). In traditional bulkwater schemes, however, raindrops can only be created through the 'autoconversion' process.

(*b*) *Microphysical processes*

The warm-cloud processes considered are cloud drop activation, drop growth by vapour diffusion, collision coalescence and break-up (see Table 1). The theories of cloud drop activation and subsequent growth by vapour diffusion are well established (cf. Pruppacher and Klett 1997), and are treated in detail in the model by Chen and Lamb. Tests have been performed against the quasi-analytical solutions of Twomey (1959), which express the maximum supersaturation $\Delta S_{\max}$ and activated cloud drop number concentration $N_{\mathrm{C,max}}$ as functions of the updraught speed W and a specific distribution of CCN. Figure 1 shows the $N_{\mathrm{C,max}}$ derived from the detailed model using the initial CCN distribution of $N_{\mathrm{CCN}} = C\Delta S^k$ (where C and k are constants) given by Twomey (1959). The result follows fairly close to Twomey's solution at k values less than about 0.4, where $N_{\mathrm{C,max}}$ generally increases with larger C and smaller k. However, at higher k values, the dependence of $N_{\mathrm{C,max}}$ on k becomes quite weak. This result is very similar to that obtained by Hegg *et al.* (1991) who also use a detailed model to calculate $N_{\mathrm{C,max}}$ but for C less than 300 cm^{-3} only. At higher C values, our result further suggests a reversal of the dependence on k when it becomes greater

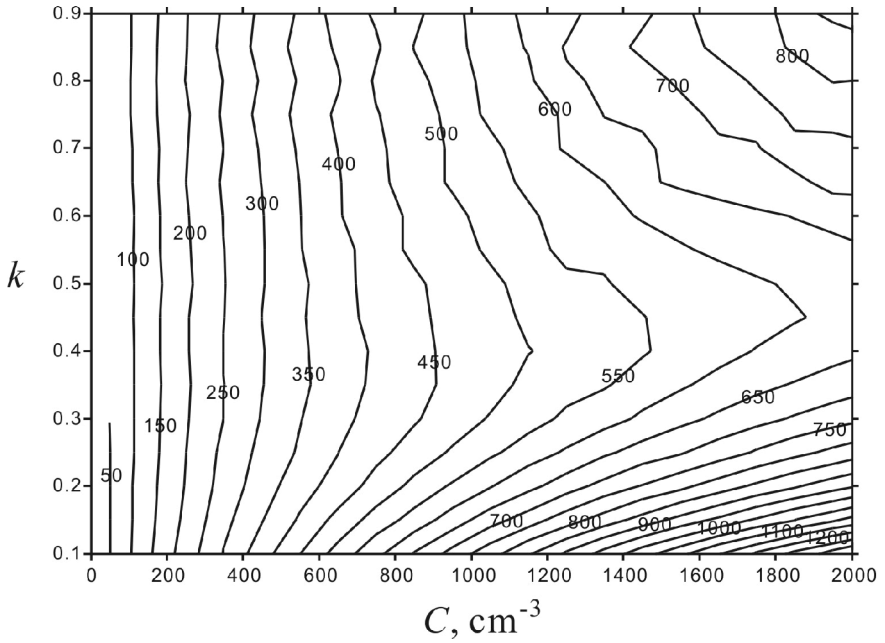

Figure 1. Model calculated number concentration of cloud drops activated from a cloud condensation nuclei distribution of $N_{CCN} = C\Delta S^k$, expressed as a function of the coefficients C and k where S is the supersaturation. The updraught speed used for this calculation is 1 m s^{-1}.

than about 0.4. The discrepancies between the results from the two detailed models and Twomey's approximate solution are most likely due to the simplification of Twomey's growth equation that ignored factors such as the solute effect and gas-kinetic effect.

The model by Chen and Lamb is upgraded to improve the calculation of hydrodynamic interactions. We adopted Böhm's (1992b) semi-analytical solution for the collision efficiency. Then, the coalescence efficiency is improved as follows. As pointed out by Hu *et al.* (1998), the large uncertainties that exist in the calculation of hydrodynamic interactions are usually due to insufficient knowledge of the coalescence efficiency. Currently, one must rely on the sparse experimental data due to the lack of analytical solutions. Low and List (1982a) conducted one of the most comprehensive investigations on the coalescence process involving pairs of large drops. They provided empirical formula for the coalescence efficiency, E_{coal}, for drop radii $r_S \geqslant 250$ μm and $r_L \geqslant 500$ μm, the smaller and larger drops, respectively. Experimental data on cloud drop-size coalescence efficiency, on the other hand, are rare. The one closest to the desired size range comes from Beard and Ochs (1984), who worked on drop pairs of $1 \leqslant r_S \leqslant 32$ μm and $50 \leqslant r_L \leqslant 500$ μm. More recently, Qian and Law (1997) performed a comprehensive study on the coalescence and break-up behaviour during droplet collision at a wide range of atmospheric pressure values as well as different gas mediums. Unfortunately, no quantitative description of E_{coal} was provided. So, for this study only the data of Low and List (1982a) for large drops and Beard and Ochs (1984) for small drops are useful. When each of these is extrapolated into the size range of the other it is in disagreement. The following equations provide a way of blending the two schemes together as shown in Fig. 2:

$$E_{coal} = E_{BO}\alpha + E_{LL}(1 - \alpha), \tag{1}$$

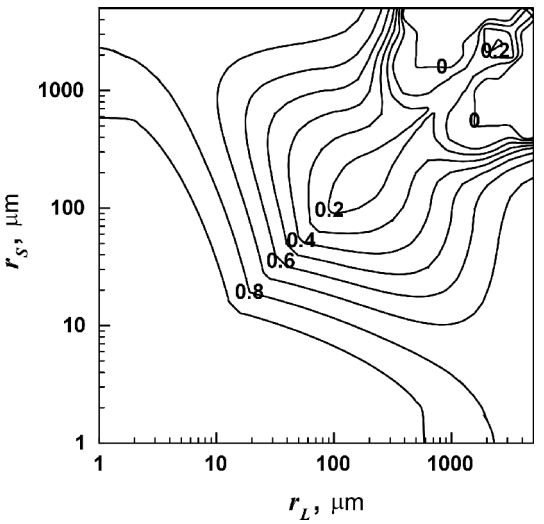

Figure 2. Coalescence efficiency between a pair of drops of radii r_L and r_S calculated from the hybrid formula Eq. (2). The contour interval is 0.1.

where E_{BO} and E_{LL} are the coalescence efficiencies reported by Beard and Ochs (1984) and Low and List (1982a), respectively. The function

$$\alpha \equiv \exp\{-0.5(r_S/r_{S0} + r_L/r_{L0})\} \tag{2}$$

is chosen such that an exponential weighting is given around the demarcation radii $r_{S0} = 50\ \mu$m and $r_{L0} = 500\ \mu$m of the two datasets. This hybrid formula produces values that are in good agreement with the original data. For the fall speed of hydrometeors we adopted formulae of Böhm (1992a), except that the flatness correction factor of Green (1975) is imposed on drops with radii $\geqslant 1$ mm.

(*c*) *Formulation of the bulk conversion rates*

To convert the results of the detailed model into bulkwater parametrizations, it is necessary to group particle properties (mixing ratio and number concentration) of the detailed model into two coarse categories as defined previously. Also, the rates of all transformations between categories in the detailed model are classified accordingly, so that statistical fitting between the bulk properties and their conversion rates can be derived. Besides using a more detailed microphysical model, we also apply a somewhat different principle implemented by Lee (1989). That is, we minimize the level of parametrization by analysing the theoretical equations, and segregate the parameters that are independent of the bulk parameters. Take the simplified equation of diffusion growth for example (cf. Pruppacher and Klett 1997):

$$\left.\frac{\mathrm{d}m}{\mathrm{d}t}\right|_{\mathrm{dif}} = \frac{4\pi r \Delta S}{A}, \tag{3}$$

where A is a function of air temperature and pressure only:

$$A \equiv \left\{ \frac{T R_v}{D_v e_{sw}} + \frac{L_v}{T k_a}\left(\frac{L_v}{T R_v} - 1\right)\right\}. \tag{4}$$

The group conversion rate for all cloud drop bins in the detailed model is then

$$\dot{Q}_{\mathrm{C,dif}} = \frac{1}{\rho_{\mathrm{a}}} \sum_i n_i \left.\frac{\mathrm{d}m_i}{\mathrm{d}t}\right|_{\mathrm{dif}} = \frac{4\pi \Delta S}{\rho_{\mathrm{a}} A} \sum_i n_i r_i \equiv B \cdot C, \tag{5}$$

where i is the bin index, n is the number density function, $B \equiv 4\pi \Delta S/(\rho_{\mathrm{a}} A)$, and $C \equiv \Sigma n_i r_i$. One can see that C is a function of the droplet properties only, while B is independent of them; so a modified bulk conversion rate can be expressed as a function of the bulk properties N_{C} and Q_{C} (or their derivatives) without carrying B in the parametrization:

$$\dot{Q}^*_{\mathrm{C,dif}} \equiv \dot{Q}_{\mathrm{C,dif}}/B = C \approx f_Q(N_{\mathrm{C}}, Q_{\mathrm{C}}), \tag{6}$$

where $f_Q(N_{\mathrm{C}}, Q_{\mathrm{C}})$ is the parametrization (fitting function) to be derived. Note that, to be more exact, ΔS actually changes slightly with the drop size due to solute and curvature effects, whereas A needs to be modified by the gas-kinetic and ventilation effects. But these size dependencies are absorbed to some degree into $f_Q(N_{\mathrm{C}}, Q_{\mathrm{C}})$ during actual parametrization. Equation (3) can also be used for the diffusion growth of raindrops. Note that in our scheme the same formula is used for both condensation and evaporation, whereas Lee (1989) used two separate formulae.

A simple analysis of Eq. (5) may be used to illustrate the importance of including number concentration in the explicit bulkwater parametrization. Figure 3 shows the relationship between the conversion rate $\dot{Q}^*_{\mathrm{C,dif}}$ and mixing ratio Q_{C} of cloud drops calculated from the detailed model. Clearly, $\dot{Q}^*_{\mathrm{C,dif}}$ is not a function of Q_{C} alone but rather, according to Eq. (5), proportional to their number concentration and radii which evolve rather differently than the mass mixing ratio. Let us take the outermost curve (corresponding to an updraught speed $W = 1.5\ \mathrm{m\ s^{-1}}$) in Fig. 3 to describe the evolution history of the two parameters. Initially, after the short activation stage at the cloud base, cloud drop number concentration remains fairly constant as the collision process is still not effective. So the growth rate increases with time only because the drops are getting larger by diffusion growth (upper left of the curve). However, due to the inverse proportionality of 'drop size growth rate' to the drop size itself, the increase in size due to diffusion growth gradually slows down, thus the change of $\dot{Q}^*_{\mathrm{C,dif}}$ becomes slower than that of Q_{C}, causing the curve to flatten out (upper right of the curve). Meanwhile, as the cloud drops get larger, collision-coalescence becomes more significant. So the self-collection among cloud drops reduces N_{C} more effectively then the increase in drop sizes. As a result, $\dot{Q}^*_{\mathrm{C,dif}}$ decreases according to Eq. (5), causing the curve to turn downward. Later, raindrops form and start to accrete cloud drops, and the reduction in N_{C} causes a decrease in both Q_{C} and $\dot{Q}^*_{\mathrm{C,dif}}$ at about the same rates. So, the evolution track follows a nearly straight line (lower part of the curve), rather different from the curvature at the earlier stage. Heading further back toward the coordinate origin, the tracks are making small circles. Such looping tracks are due to the reactivation of interstitial (previously non-activated) aerosol particles into new cloud drops, which repeats the aforementioned evolution but much faster because of the existing droplets. More details of this reactivation process are discussed in subsection 4(b).

A linear fitting of $\dot{Q}^*_{\mathrm{C,dif}}$ in Fig. 3 as a function of Q_{C} gives a coefficient of determination (r^2) of 0.79, which is similar to that ($r^2 = 0.81$ or $r = 0.9$) given by Lee (1989). These r^2 values reflect the inherent limitation of a one-moment parametrization. Parametrizations for other processes also have similar problems. Significant improvement is achieved by considering a second moment of the drop size distribution, the

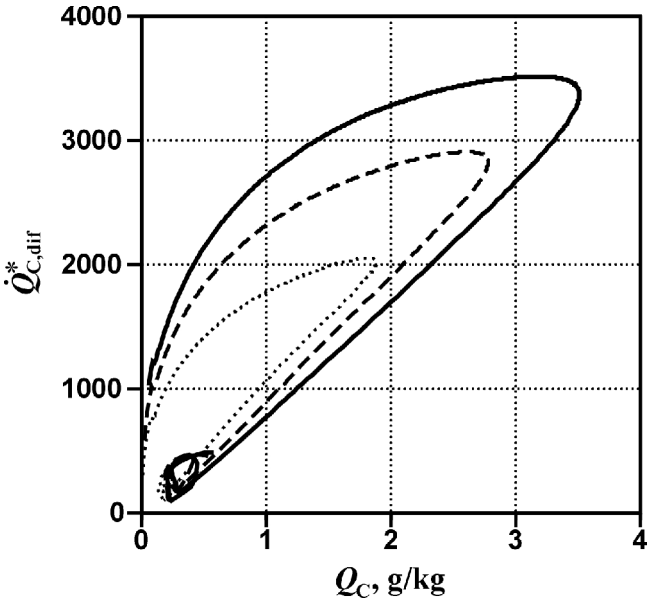

Figure 3. Relationship between the conversion rates $\dot{Q}^*_{C,dif}$ and mixing ratios Q_C for the diffusion growth of cloud drops from a parcel simulation with a detailed bin model. The three curves (from inside out) correspond to updraught speeds of 0.5, 1.0 and 1.5 m s^{-1}.

most obvious choice of which is the number concentration. Figure 4 shows the same conversion rate $\dot{Q}^*_{C,dif}$ as shown in Fig. 3 but now it is plotted against both the mass mixing ratio and number concentration. The fitting function $f_Q(N_C, Q_C)$ in Eq. (3) is shown as the shaded surface. With an additional moment, the model results can now be fitted with a much improved coefficient of determination of $r^2 = 0.97$. Note that one may use the combinations of the moments as parameters to the fitting function, such as using the mean volume radius, r_C, to replace Q_C, where

$$r_C \equiv \left(\int r_d^3 n(r_d)\, dr_d \Big/ \int n(r_d)\, dr_d \right)^{1/3} = (3Q_C \,/ 4\pi\rho_w N_C)^{1/3}. \tag{7}$$

In so doing, the correlation can be improved slightly to $r^2 = 0.99$ for the data shown in Fig. 4. This improvement, although minor in this case, indicates the more direct connection of the conversion rate $\dot{Q}_{C,dif}$ to drop radius than mass mixing ratio, as is evident from Eq. (5).

The hydrodynamic interactions can be expressed with the stochastic collection equation:

$$\frac{\partial n(x)}{\partial t} = \frac{1}{2} \int_{x1}^{x2} K(x - y, y) n(x - y) n(y)\, dy - n(x) \int_{y1}^{y2} K(x, y) n(y)\, dy \tag{8}$$

where $K(x, y)$ is the collection kernel between drops with masses x and y. The group conversion rate for all bins in the detailed model is then

$$\dot{N}_{col} = \frac{1}{\rho_a} \sum_i \frac{\partial n_i(x)}{\partial t}. \tag{9}$$

Now, in the collection kernel

$$K(x, y) = \pi (r_x + r_y)^2 E(x, y) |U(x) - U(y)|, \tag{10}$$

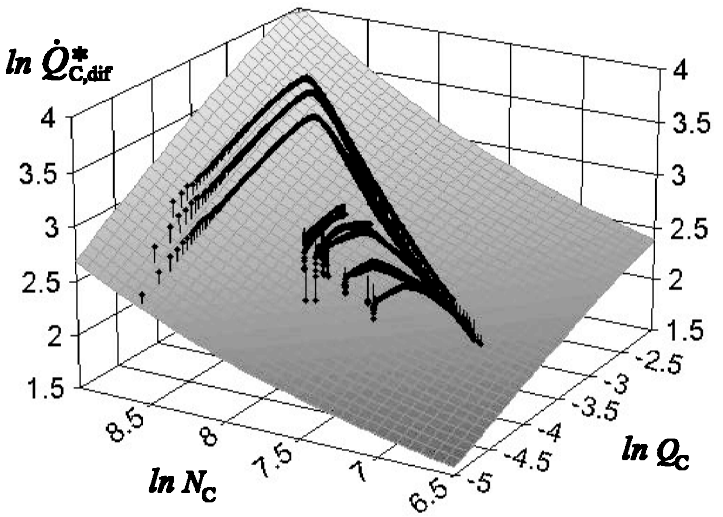

Figure 4. Conversion rate $\dot{Q}^*_{C,dif}$ plotted as a function of cloud drop bulk mass Q_C and number concentration N_C. Residuals between the model result (dotted symbols) and regression result (shaded surface) are indicated by the vertical bars.

TABLE 1. PROGNOSTIC FORMULAE FOR THE BULK CONVERSION RATES OF VARIOUS MICROPHYSICAL PROCESSES

Item	Process	Parametrization formula
1	Diffusion growth of cloud drops	$\dot{Q}_{C1} = \Delta S/A \cdot \exp(a + b \cdot \ln N_C + c \cdot \ln r_C)$
2	Diffusion growth of raindrops	$\dot{Q}_{R2} = \Delta S/A \cdot N_R \exp\{a + b \cdot (\ln r_R)^2 + c \cdot (\ln r_R)^3\}$
3	Cloud drop self-collection	$\dot{N}_{C3} = -\exp\{a + b \cdot \ln N_C + c \cdot (\ln r_C)^3\} \cdot g(r_C, \rho_a)$
4	Autoconversion (cloud drop self-collection and formation of raindrops)	$\dot{N}_{C4} = -N_C^2 \cdot \exp(a + b \cdot r_C + c/r_C) \cdot g(r_C, \rho_a)$ $\dot{N}_{R4} = -\dot{N}_{C4}$ $\dot{Q}_{C4} = \dot{N}_{C4} \cdot \exp(a + b \cdot Q_C/N_C)$ $\dot{Q}_{R4} = -\dot{Q}_{C4}$
5	Accretion of cloud drops by raindrops	$\dot{N}_{C5} = -N_C \cdot N_R \cdot \exp(a + b \cdot \ln r_R + c \cdot \ln r_C) \cdot g(r_R, \rho_a)$ $\dot{Q}_{C5} = -N_C \cdot N_R \cdot \exp(a + b \cdot \ln r_R + c \cdot \ln r_C) \cdot g(r_R, \rho_a)$ $\dot{Q}_{R5} = -\dot{Q}_{C5}$
6	Raindrop self-collection	$\dot{N}_{R6} = -\exp(a + b \cdot \ln N_R + c/r_R) \cdot g(r_R, \rho_a)$
7	Raindrop formation from the collision-break-up of raindrops	$\dot{N}_{R7} = -\dot{N}_{R6} \cdot \exp\{a + (b + c \cdot r_R) \cdot r_R\}$
8	Cloud drop formation from collision-break-up of raindrops	$\dot{N}_{R8} = \dot{N}_{R6} \cdot \exp\{a + (b + c \cdot r_R) \cdot r_R\}$ $\dot{N}_{C8} = -\dot{N}_{R8}$ $\dot{Q}_{C8} = \exp(a + b \cdot \ln \dot{N}_{C8} + c \cdot \ln r_R)$ $\dot{Q}_{R8} = -\dot{Q}_{C8}$
9	Cloud drop deactivation	$\dot{N}_{C9} = -\exp\{a + b \cdot \ln N_C + c \cdot \ln r_C + d \cdot \ln(-\Delta S)\}$ $\dot{Q}_{C9} = \dot{N}_{C9} \cdot 4.1888 \times 10^{-15}$
10	Cloud drop formation from raindrop evaporation	$\dot{N}_{R10} = \Delta S \cdot A \cdot \exp(a + b \cdot \ln N_R + c \cdot \ln r_R)$; $\dot{N}_{R10} \leqslant 0$ $\dot{Q}_{R10} = \dot{N}_{R10} \cdot 5.236 \times 10^{-10}$ $\dot{N}_{C10} = -\dot{N}_{R10}$; $\dot{Q}_{C10} = -\dot{Q}_{R10}$
11	Auxiliary functions for terminal velocity adjustment	$f(r_d, \rho_a) = \exp[\exp\{a + b \cdot (\ln r_d)^3 + c \cdot (\rho_a)^{1.5}\}]$ $g(r_d, \rho_a) = f(r_d, \rho_a) \cdot \rho_a$

Coefficient A in items 1 and 2 is defined in Eq. (4).

where r_x and r_y are radii of drops with masses x and y. The collection efficiency E and terminal velocity U both depend on the ambient air properties T and P. However, such dependence is either difficult to formulate or simply not well-known. We did not attempt to separate out the dependencies on T and P completely as was done in Eq. (6). Instead, a surrogate variable—air density—is used to account for these dependencies, which is a common practice in many bulkwater schemes. As a result, the bulk conversion rates for the collision-coalescence processes are now simplified as:

$$\dot{N}_{\mathrm{X,col}} \approx f_N(N_\mathrm{Y}, N_\mathrm{Z}, Q_\mathrm{Y}, Q_\mathrm{Z}) \cdot g, \tag{11}$$

where X, Y, and Z represent the resulting drop group, the collector drop group, and the collected drop group, respectively, and g represents the effect of air properties on the collision kernel expressed as a function of air density. Similarly, the change of drop mass mixing ratio due to the collision processes can be written as:

$$\dot{Q}_{\mathrm{X,col}} \approx f_Q(N_\mathrm{Y}, N_\mathrm{Z}, Q_\mathrm{Y}, Q_\mathrm{Z}) \cdot g. \tag{12}$$

All collision-related processes can be expressed in similar forms to Eqs. (11) and (12). We list these six processes as items 3 to 8 in Table 1.

3. Bulk parametrization

After establishing the basic mathematical forms of the conversion rates, the bulk parameters Q and N as well as the bulk conversion rates $\dot{Q}$ and $\dot{N}$ are generated using a Lagrangian air parcel model with Chen and Lamb's (1994) microphysics and the improvements mentioned above. Curve-fitting software is then used to obtain the parametrization functions f_Q, f_N and g. In the following we discuss the experimental set-up and the parametrization formulae derived.

(*a*) *Experimental design*

In order to ensure the applicability of the parametrization scheme to all possible situations, it is necessary to generate a large dataset by running the detailed model under a broad range of conditions. One can run the detailed model in simple (i.e. parcel model) or complicated (multi-dimension model) ways. Here we choose to run it as a parcel model to: (i) save computational time; (ii) have more control on the possible outcomes; (iii) avoid artificial interference from the dynamic processes, such as advection and mixing, on the microphysical processes (more on this point will be discussed in section 5); and (iv) avoid numerical errors associated with advection in a multi-dimensional spatial domain. We argue that because the present parametrization is performed on instantaneous conversion rates in an air parcel, it is readily applicable in dynamic models, so long as turbulence closure is properly included.

The most important factors considered in designing the scenarios for detailed simulation are: the effects of aerosol size distribution, broad ranges of cloud water and rain-water contents, together with the relative occurrence of each microphysical process and the value-range of its dependent variables. Therefore, scenarios with various aerosol size distributions, updraught speeds, and cloud-base conditions (temperature and pressure) are designed to increase the range of applicability and statistical meaning of the results. We selected seven types of aerosol size distributions, with types 1 to 5 from Whitby (1978) comprising: (i) marine surface background, (ii) clean continental background, (iii) average background, (iv) urban average, and (v) background and local sources; and types 6 and 7 from Jaenicke (1993) comprising: (vi) maritime, and

TABLE 2. COEFFICIENTS OF THE FORMULAE IN TABLE 1 AND THE VARIANCE r^2 OF THE FITTING

Item	a	b	c	d	r^2
1	6.6793E+0	1.0090E+0	1.4095E+0	–	0.9988
2	9.9912E+0	−4.7678E+0	−3.1388E−2	–	0.9656
3	−4.3561E+0	1.9934E+0	1.6465E−2	–	0.7453
4	−4.0731E+1	5.3720E+5	−2.0139E−5	–	0.6833
	−2.1370E+1	1.9899E+9	–	–	0.9978
5	1.5519E+1	3.1491E+0	4.3989E−1	–	0.9797
	2.0090E+1	2.9626E+0	3.2358E+0	–	0.9949
6	−1.8239E+1	2.2956E+0	−2.3261E−4	–	0.8531
7	−1.7431E+2	2.6031E+5	−9.3613E+7	–	0.7074
8	−1.6185E+2	2.2786E+5	−7.6988E+7	–	0.7557
	−2.3531E+1	9.8271E−1	−1.3202E−1	–	0.9969
9	−1.0593E+0	8.9774E−1	−2.8403E−1	1.6328E+0	0.6196
10	8.2841E+0	9.7219E−1	−5.0808E−1	–	0.7583
11	3.1250E−1	1.0552E−3	−2.4023E+0	–	0.9850

The number of significant figures is chosen such that any less would cause significant precision error.

(vii) remote continental, which are quite different from those of Whitby. Each aerosol number density function is represented by three log-normal distributions (representing the commonly understood definitions of the nuclei mode, accumulation mode and coarse mode aerosols), and their chemical activities are assumed to be equivalent to that of an ammonium sulphate solution. For the conditions of cloud formation, we used two cloud-base conditions (900 hPa, 15 °C; and 700 hPa, 0 °C), and five constant updraught speeds ($W = 0.2$, 0.5, 1, 2, and 5 m s^{-1}). Additional simulations with varying (sinusoidal) updraught speeds are designed to allow the air parcel to descend to its original height. In this way the evaporation and deactivation of cloud drops and raindrops can be accounted for. For these simulations, the set-up of aerosol size distribution remains the same, but the initial relative humidities are 70%, 80% and 90%, and the maximum values of the sinusoidal updraughts are 0.5, 1, 2 and 3 m s^{-1}. With the aforementioned set-up over 230 simulations were performed in generating our datasets.

(*b*) *Prognostic formulae*

The microphysical processes and the prognostic formulae from regression analyses are listed in Table 1, whereas the coefficients for these formulae and their r^2 values are given in Table 2. Note that processes 1 and 2 do not affect the number concentration, whereas the mixing ratio is not affected by processes 3, 6 and 7. Also note that raindrop formation by autoconversion is considered to proceed in two steps: self-collection of cloud drops (remove one cloud drop) by process 3, and then turning coalesced drops that exceed the size threshold into a raindrop by process 4 (remove another cloud drop).

Most of the fittings have r^2 greater than 0.95, indicating that the statistical two-moment parametrization should produce bulkwater properties very close to those of the detailed model. The ones that do not have high correlations are cloud drop self-collection, autoconversion, raindrop self-collection, collision break-up-related processes, and evaporation-related processes. The lowest r^2 (0.62) is in the fitting of cloud drop deactivation during evaporation (supposed return to aerosol population). These low-r^2 processes have one thing in common: their conversion rates depend on the width of the actual size distribution, which cannot be retrieved from a two-moment scheme.

As mentioned earlier, not all formulae are expressed in terms of the two moments Q and N. Very often r_C is used instead of Q_C to get a simpler formula of higher accuracy. Note that many of the processes in Table 1 have rather linear dependencies on the number concentrations with respect to each of the bulk categories involved. For these situations, we simply adopt linear dependence (for non self-collision processes 2 and 5), or square dependence (for self-collection process 4) to make the fitting of other parameters an easier job. Also, we found that it is sometimes desirable to adopt other conversion rates in the formulation when the two processes are highly related, such as embedding $\dot{N}_{C4}$ in $\dot{Q}_{C4}$ and $\dot{N}_{R6}$ in both $\dot{N}_{R7}$ and $\dot{N}_{R8}$.

Detailed examination of the parametrization formulae may not only ensure their effectiveness but also give more insight into the physics. For example, process 1 in Table 1 shows that the condensation rate is almost linearly proportional to N_C (while holding the second variable constant) and to the 1.4 power of r_C. However, Eq. (5) seems to indicate a linear dependence on both N_C and r_C. The stronger dependence on r_C partly results from the solute, curvature, gas-kinetic and ventilation effects that were considered in the detailed model. All these effects favour the growth of larger drops (and thus contribute to a stronger dependence on r_C): the gas-kinetic effect retards the condensation more for smaller drops; the solute effect is stronger for larger drops, which normally have higher solute concentration; the ventilation effect is stronger for larger drops with higher fall speeds. Also note that r_C in Table 1 is the mean volume radius, whereas the r_i in Eq. (5) corresponds to a mean number radius.

A microphysical process that is often crudely represented in traditional bulkwater schemes is the so-called 'autoconversion', a term typically used to describe the production of a raindrop through cloud drop coalescence. Kessler (1967) applied a Heaviside function in the autoconversion equation, such that the conversion is turned on abruptly when the cloud drop mixing ratio exceeds a critical value, Q_{crit}. This abrupt turn-on by the Heaviside function is artificial, and the selection of the critical value is subjective, so larger uncertainties may be expected. In reality, the autoconversion rate does not depend directly on the cloud water content, but rather on the drop sizes and the dispersion of the drop sizes, because it proceeds mainly via collision-coalescence. Berry and Reinhardt (1973) improved the autoconversion formula by treating it as a function of the mean and dispersion of cloud drop sizes (masses), whereas Tripoli and Cotton (1980) adopted this concept and modified their scheme to include the simplified droplet spectral broadening effect, yet still retain the Heaviside function in their autoconversion formulae. We wish to note that such improvements cannot be made without the additional information of the number concentration. Indeed, our formula (item 4) in Table 1 shows a strong dependence of the autoconversion rate on both N_C and r_C. However, the spectral dispersion that strongly influences the autoconversion process cannot be described explicitly with a two-moment scheme, which is part of the reason why the r^2 of this parametrization is not particularly high. The dependence on the square of N_C is a typical characteristic of a collision process, whereas the dependence on r_C is quite nonlinear and requires further discussions. Khairoutdinov and Kogan (2000) demonstrated with their bin model that the autoconversion rate is proportional to the mean volume radius raised to the power of 5.7. Replacing with a log-linear fit, our results would give a dependence that is raised to the power of 7.7, which is significantly stronger than that reported by Khairoutdinov and Kogan. Such a strong dependence indicates a sharp gradient that more or less echoes the use of a Heaviside function by Kessler (1967). Nevertheless, one should use a critical drop size, r_{crit}, as did Berry and Reinhardt (1973) rather than the Q_{crit} used by Kessler (1967). Furthermore, sometimes an autoconversion rate that is negligible for convective clouds can still be significant for shallow clouds in which the cloud water content

TABLE 3. DIAGNOSTIC FORMULAE GENERATED FROM THE PHYSICAL–STATISTICAL METHOD

Item	Diagnostic variable	Parametrization formula
1	Cloud drop sedimentation flux	$FN_C = \exp(a + b \cdot \ln N_C + c \cdot \ln r_C) \cdot g(r_C, \rho_a)$ $FQ_C = \exp(a + b \cdot \ln N_C + c \cdot \ln r_C) \cdot g(r_C, \rho_a)$
2	Raindrop sedimentation flux	$FN_R = \exp(a + b \cdot \ln N_R + c \cdot \ln r_R) \cdot g(r_R, \rho_a)$ $FQ_R = \exp(a + b \cdot \ln N_R + c \cdot \ln r_R) \cdot g(r_R, \rho_a)$
3	Cloud drop group fall speed	$U_C = \{a + (b + c \cdot r_C) \cdot r_C\} \cdot r_C \cdot f(r_C, \rho_a)$
4	Raindrop group fall speed	$U_R = \exp\{a + (b + c/r_R)/r_R\} \cdot f(r_R, \rho_a)$
5	Logarithmic radar reflectivity	$\mathrm{dB}Z_R = a + b \cdot \ln(N_R) + c \cdot \ln(r_R)$
6a	Cloud drop effective radius	$r_{e,C} = \exp(a + b \cdot \ln N_C + c \cdot \ln r_C)$
6b		$r_{e,C} = \exp(a + b \cdot \ln N_C + c \cdot \ln Q_C)$
7	Raindrop effective radius	$r_{e,R} = \exp(a + b \cdot \ln N_R + c \cdot \ln r_R)$
8a	Ratio of $r_{e,C}$ to r_C	$\beta_C = a + b \cdot \varepsilon + c \cdot \gamma$
8b		$\beta_C = \exp(a + b \cdot \varepsilon + c \cdot \ln \sigma)$
9	Standard deviation of cloud drop size distribution	$\sigma = \exp(a + b \cdot \ln N_C + c \cdot \ln Q_C)$
10	Cloud drop mean number radius	$\overline{r}_d = \exp(a + b \cdot \ln N_C + c \cdot \ln Q_C)$

Functions g and f are defined in Table 1.

(or drop sizes) is often below or near the commonly used critical values and cloud lifetime is long. In such shallow clouds precipitation development is not only determined by the liquid water content but also the available time for rain initiation. As pointed out by Feingold *et al.* (1996), the development of drizzle in marine stratiform clouds, which is thought to have an important climatological effect (Albrecht 1989; Stevens *et al.* 1998), is strongly related to the in-cloud residence time. Such an effect cannot be resolved accurately by the traditional autoconversion formulae.

(c) *Diagnostic formulae*

Our statistical approach can also be used to generate diagnostic formulae for parameters that are important to cloud microphysical or radiative calculations. Table 3 lists formulae for the number and mass sedimentation fluxes, group fall velocity, radar reflectivity factor, effective radius, as well as a few factors that are related to the determination of the effective radius. The coefficients and r^2 of these fitting formulae are given in Table 4. Group fall velocity is a parameter required in traditional bulkwater schemes to account for the sedimentation of condensed water. For our two-moment scheme we need to provide the sedimentation flux (or group fall velocity) not only for the water mass but also the number concentration. Our formulae show that the mass flux has a stronger dependence on the particle size than the number flux, and this would produce the effect of sedimentation sorting such that larger drops tend to reside in the lower part of the clouds.

Radar reflectivity factor Z (cf. Doviak and Zrnic 1984) is a useful parameter for model validation with radar observations. In Table 3 the logarithmic radar reflectivity factor $\mathrm{dB}Z(\equiv 10 \log_{10} Z)$ can be converted back to Z with the following proportionality: $Z \propto N_R^{b'} \cdot r_R^{c'}$, where $b' = \alpha b$, $c' = \alpha c$ and $\alpha = 0.1 \cdot \ln 10$. The resulting coefficients ($b' = 1.06$ and $c' = 4.82$) indicate that Z depends almost linearly on the raindrop number concentration, and is proportional to the mean volume radius r_R raised to the power of 4.82. However, for the widely used Marshall–Palmer distribution, Z is proportional to r_R raised to the sixth power. Our weaker dependence may be due to the fact that a realistic raindrop population lacks the largest drops (of a few millimetres radius) that are described by the Marshall–Palmer distribution under high rain-water contents.

TABLE 4. COEFFICIENTS OF THE FORMULAE LISTED IN TABLE 3, AND THE EXPLAINED VARIANCE (r^2) OF THE FITTINGS

Item	a	b	c	r^2
1	1.8276E+1	1.0015E+0	1.9838E+0	0.9997
	2.0901E+1	9.9111E−1	4.4182E+0	0.9945
2	9.4791E+0	9.7607E−1	1.0858E+0	0.9928
	1.5943E+1	1.1898E+0	4.0073E+0	0.9975
3	8.8462E+2	9.7593E+7	−3.4249E+11	0.9836
4	2.1454E+0	−2.2812E−4	2.9676E−9	0.9835
5	1.2504E+2	3.9174E+0	1.7533E+1	0.8753[a]
	1.3578E+2	4.7262E+0	1.9909E+1	0.9204[b]
	1.4478E+2	5.6082E+0	2.2128E+1	0.9443[c]
6a	−1.2560E+0	−1.7904E−2	8.5536E−1	0.9365
6b	−3.5840E+0	−3.0510E−1	2.8698E−1	0.9439
7	−9.9216E−2	2.9490E−2	9.9238E−1	0.9911
8a	8.9594E−1	8.1692E−1	3.7240E−3	0.8759
8b	−4.2562E−1	6.6048E−1	−2.7135E−2	0.9041
9	−6.2685E+0	−2.7312E−1	2.2606E−1	0.5288
10	−2.2920E+0	−3.5158E−1	3.4708E−1	0.9527

Note: in item 5, each formula fits only those data with (a) $\mathrm{dB}Z > 20$, (b) $\mathrm{dB}Z > 0$, and (c) $\mathrm{dB}Z > -20$.

These large drops break up quite readily by collision as indicated by many observational studies (e.g. Willis 1984) and model results (e.g. Valdez and Young 1985; Chen and Lamb 1994) strictly for warm clouds. Note that the coefficient c' increases when we take progressively smaller lower limits of $\mathrm{dB}Z$ for the fitting (Table 4), implying the size distribution is more like that of Marshall–Palmer for lighter rain.

The effective radius, r_e, is important in determining the cloud radiative effects (Stephens 1978). It is common practice in many global or regional models to simply fix the value of r_e (e.g. Fowler *et al.* 1996; Giorgi *et al.* 1999; Gong and Wang 2000) or diagnose it from either temperature or cloud water content with assumed number concentration (e.g. Kiehl 1994; Del Genio *et al.* 1996; Lohmann *et al.* 1999). More advanced schemes convert liquid water content into r_e through the use of empirical or semi-analytical formulae (e.g. Fouquart *et al.* 1990; Moeng and Curry 1990). Yet, most observations indicated that r_e is a function of both the liquid water content and number concentration (Blyth and Latham 1991; Pontikis and Hicks 1992; Martin *et al.* 1994). Table 3 lists several diagnostic formulae that may help the understanding of aerosol effects on r_e, and a few other parameters related to the size distribution of cloud drops.

The effective radius r_e is not the same as the mean volume radius r_C defined in Eq. (7):

$$r_e \equiv \int r_d^3 n(r_d)\, dr_d \Big/ \int r_d^2 n(r_d)\, dr_d. \tag{13}$$

Using r_C in place of $r_{e,C}$ may result in significant discrepancies in the optical properties of clouds. Hereafter we will discuss the differences in terms of their ratios $\beta_C (\equiv r_{e,C}/r_C)$. Martin *et al.* (1994) showed that β_C (equivalent to their $k^{-1/3}$) is smaller for maritime air masses (1.08) than for continental air masses (1.14). By using $r_{e,C}$ from formula 6a in Table 3 and dividing it by r_C, one may obtain

$$\beta_C \propto N_C^{-0.018} \cdot r_C^{-0.145}. \tag{14}$$

At a first glance it seems that β_C from our parcel simulations decreases with increasing number concentration, which seems to be inconsistent with the reports of Martin *et al.* (1994) and Liu and Daum (2002). However, analysis of the aerosol indirect effects should be made under conditions with similar cloud water contents. By converting r_C back to Q_C and N_C with Eq. (7), we have

$$\beta_C \propto N_C^{0.030} \cdot Q_C^{-0.048}. \tag{15}$$

It now shows consistency with the observations, at least qualitatively. Incidentally, formula 6b in Table 3 produces values of β_C almost exactly the same as those reported by Martin *et al.* (1994; i.e. maritime $\beta_C = 1.08$, continental $\beta_C = 1.14$) if one uses the mean cloud drop concentrations (maritime $N_C = 50\,\mathrm{cm}^{-3} \sim 50\,\mathrm{mg}^{-1}$, continental $N_C = 400\,\mathrm{cm}^{-3} \sim 400\,\mathrm{mg}^{-1}$) from Martin *et al.* and a liquid water content of 0.3 g kg^{-1} that is typical of marine stratocumulus clouds. So our formula is also quantitatively consistent with the observational results.

Liu and Daum (2002) suggested that *Twomey's first indirect effect* of aerosol on atmospheric radiation fluxes due to increasing drop number concentration may be partially offset by an accompanying increase in β_C. Indeed, our result in Eq. (15) agrees with them. Note that in Eq. (15) the power-law dependence of $r_{e,C}$ on N_C is one-ninth weaker in magnitude than that of r_C (note: $r_C \propto N_C^{-1/3}$ at fixed Q_C). So our results further suggest that the increase of β_C may offset about one-ninth of the *first indirect effect*. However, an increase of cloud drop number concentration may also lead to the *second indirect effect* that follows with enhanced cloud lifetime and cloud water content due to weakened collisions and suppressed precipitation (Albrecht 1989; Rosenfeld 2000). As Eq. (15) also suggests a decrease of β_C with increasing cloud water content, we suspect that the *second indirect effect* may to some extent counterbalance the influence of β_C on the *first indirect effect*. The extent to which these two indirect effects offset each other is left for the dynamics, which drives the water transport, to decide.

If we were to parametrize β_C directly with N_C and r_C (instead of getting $r_{e,C}$ first and then dividing it by r_C), the r^2 would be quite low (about 0.23) because the primary dependence (on r_C) has been largely removed. Theoretically, as pointed out by Martin *et al.* (1994), β_C depends primarily on the spectral dispersion ε and somewhat on the skewness γ of the drop size distribution, and should be independent of N_C. The above parameters are defined as:

$$\varepsilon \equiv \sigma / \overline{r}_d, \tag{16}$$

$$\gamma \equiv (1/\sigma^3 N_C) \int (r_d - \overline{r}_d)^3 n(r_d)\, dr_d, \tag{17}$$

where σ is the standard deviation and $\overline{r}_d$ is the mean number radius:

$$\sigma \equiv \left\{ (1/N_C) \int (r_d - \overline{r}_d)^2 n(r_d)\, dr_d \right\}^{\frac{1}{2}}, \tag{18}$$

$$\overline{r}_d \equiv (1/N_C) \int r_d n(r_d)\, dr_d. \tag{19}$$

According to item 8a in Tables 3 and 4, it seems that β_C can be fitted quite well simply with ε and γ. In that case, where is the dependence of β_C on N_C in Eq. (15) coming from? Actually, the components of ε (i.e. $\overline{r}_d$ and σ) both depend on N_C and Q_C. The behaviour of $\overline{r}_d$ is similar to that of r_C, becoming smaller with greater N_C

at fixed Q_C. As for σ, it also decreases with increasing N_C (see item 9 in Tables 3 and 4), a result consistent with the report of Alkezweeny *et al.* (1993). However, the much stronger effect of $\overline{r}_d$ on β_C (proportional to N_C raised to about one-third power) surpasses that of σ (proportional to N_C raised to the –0.27 power according to item 9 in Tables 3 and 4). So, while Liu and Daum (2002) reasoned that the increase in β_C with higher N_C is mainly due to the increase of the dispersion ε, we further propose that the increase of ε is mainly a result of the reduction in $\overline{r}_d$. As for the other dependent variable (γ) that may theoretically affect β_C, we could not find a significant correlation of it to either N_C or Q_C. Actually, β_C can be fitted even better with ε and σ (item 8b in Tables 3 and 4), suggesting the role of γ should be quite minor.

(*d*) *The activation size*

Judging from the high precision (r^2) of the diffusion growth rate formulae (Table 2), our parametrization scheme should be able to calculate accurately the supersaturation and cloud drop number concentration at given updraught speeds. However, an initial size (mass) of the activated drop must be given when implementing the formulae in Table 1, otherwise the droplets will not grow. Bulk parametrization schemes normally do not track the thermodynamic and chemical states of aerosol particles before activation, so one does not actually know this activation size. With some sensitivity tests we further found that the overall cloud drop number concentration is rather sensitive to this activation size, because it influences the overall diffusion growth and thus the ambient supersaturation. One might think of using the equilibrium size of aerosol particles at 100% relative humidity (at the cloud base), or the critical size of activation as determined by the Köhler theory. The equilibrium size at 100% saturation, r_0, can be derived from the simplified Köhler equation (cf. Pruppacher and Klett 1997):

$$S_{eq} \approx 1 + \frac{a}{r_d} - \frac{b}{r_d^3}, \tag{20}$$

by letting $S_{eq} = 1$, which gives

$$r_0 = \sqrt{b/a}. \tag{21}$$

The problem is that, as the air properties constantly change in the updraught, the particles might not adjust their sizes fast enough to the new conditions and reach the Köhler-theory equilibrium.

Figure 5 shows the swelling ratio (wet size to dry size) of ammonium sulphate particles as a function of the dry size and ambient relative humidity (cf. Chen 1994b). One can see that in an updraught just reaching the cloud base (i.e. an air parcel just reaching 100% saturation), the actual particle sizes (solid curves) are significantly smaller than the equilibrium sizes for particles with dry sizes roughly greater than 0.1 μm. Two factors contribute to such differences: firstly, larger particles have much longer characteristic times of diffusion growth (proportional to the square of size); secondly, the size dependence of the equilibrium swelling factor changes dramatically near 100% saturation. At well below 100% saturation the curvature effect is much smaller than the solute effect for particles with r_{dry} greater than about 0.1 μm, such that the swelling factor does not vary significantly with the particle size. On the other hand, one can see from Eq. (21) that at $S_{eq} = 1$ the swelling factor is proportional to the square root of r_{dry}, where $r_{dry} \propto b^{1/3}$. So the size-dependence of the swelling factor at $S_{eq} = 1$ deviates significantly from the other equilibrium curves in Fig. 5. For a 1 μm dry size, the equilibrium size is about four times larger than the actual size; for a 10 μm

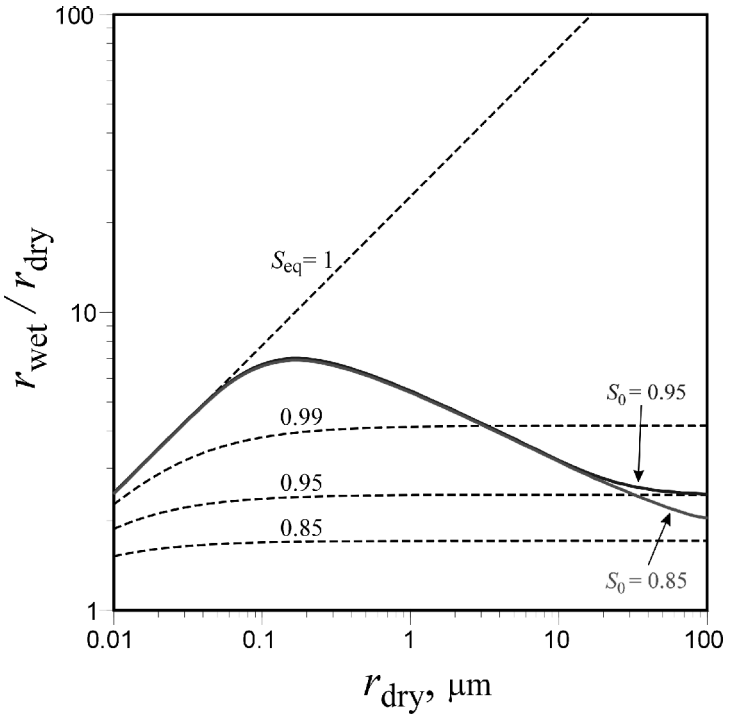

Figure 5. Swelling ratios (wet radius/dry radius) of ammonium sulphate particles as a function of the dry radius. The dashed curves are for particles in thermodynamic equilibrium with the ambient air at saturation ratios, S_{eq}, of 0.85, 0.95, 0.99 and 1.00. The solid curves are the instantaneous swelling factor for particles growing at a constant updraught of 1 m s^{-1} at the instant when the air parcel has just reached 100% saturation; the values arrowed at the end of these curves indicate the initial saturation ratio, S_0, of that air parcel. The instantaneous curves deviate significantly from the equilibrium curve (100% saturation) for particles with a dry size greater than about 0.1 μm.

dry size the difference rapidly increases to over 20 fold. It would be erroneous to use r_0 hastily to represent the activation size. The Köhler-curve critical radius is an even worse choice because it is $\sqrt{3}$ times r_0.

To solve this problem, we generated a formula for the activation size r_{act} by a statistical fitting of results from the detailed model:

$$r_{act} = r_0 \cdot 10^{a+b\cdot X+c\cdot X^2} \cdot W^d, \tag{22}$$

where $X = \log_{10}(r_{dry})$, and the fitting coefficients $a = -0.61425$, $b = -0.66625$, $c = -0.17368$, and $d = -0.11782$. Note that the stronger the updraught, the farther a particle deviates from its equilibrium size as indicated by the last term of Eq. (22). One may notice in Fig. 5 that the initial relative humidity also influences actual sizes at the cloud base (at 100% saturation) for particles with large dry sizes ($r_{dry} > 20$ μm). Those started at lower relative humidity deviate more from their equilibrium sizes after a longer ascending time; however, we ignored this memory effect because it is limited to very large aerosols and is not strong enough to affect the overall activation process significantly.

(*e*) *Rain embryo*

With the determination of the activation sizes, our scheme also allows the formation of raindrops immediately at the cloud base by putting giant nuclei with $r_{act} > 50$ μm

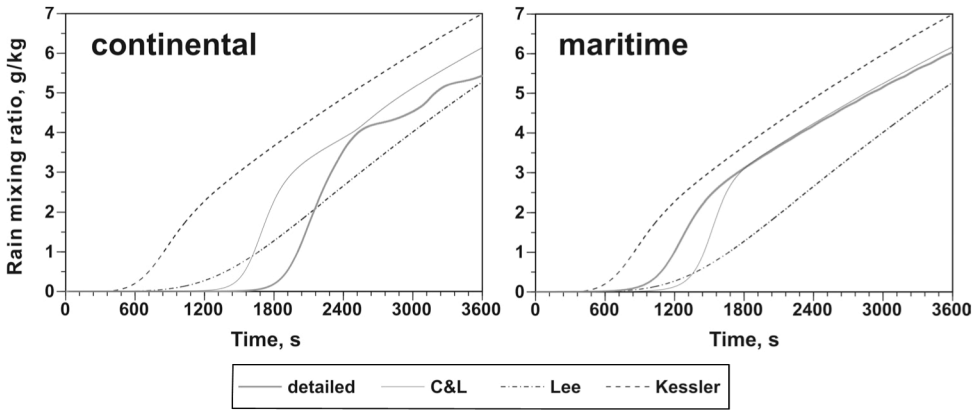

Figure 6. Comparison of the rain-water contents simulated with the detailed model and three other parametrization schemes for the continental and maritime aerosol scenarios. The simulations were run in a parcel model with a constant updraught of 1 m s^{-1}. See text for details.

into the rain category. Moreover, to compensate for the inaccuracy in the autoconversion parametrization, we regard some of the smaller giant nuclei as rain embryos, and also put them straight into the raindrop category. By doing this, the dependence of the autoconversion rate on the dispersion of the drop size distribution is partially accounted for. We found that the initiation of rain can be improved significantly by letting all condensation nuclei with $r_{\mathrm{dry}} > 10\ \mu$m be activated as raindrops directly (discussion on the sensitivity of the value of r_{dry} is given in subsection 4(a)). Note that we took the same measure during the re-grouping of droplets for detailed model output, by counting drops with $r_{\mathrm{dry}} > 10\ \mu$m as raindrops. Therefore the rate equations derived for raindrops may be extrapolated to these 'rain embryos' although they do not yet have a 50 μm radius.

4. Comparison with other schemes

The parametrization set in Table 1 (based on Chen and Lamb (1994,1999) and hereafter called the C&L scheme) was tested against the detailed model as well as other bulkwater schemes by simulations in parcel mode. Here we first demonstrate how the C&L scheme responds to a change in the input aerosol. Note that Kessler's (1967) and Lee's (1989) schemes do not respond to aerosol input.

(*a*) *Rain-water development*

Figure 6 shows the development of rain water in an air parcel ascending with a constant updraught speed of 1 m s^{-1} using all three schemes, and corresponding to the continental and maritime aerosol types of Whitby (1978). Although the general trends are similar, significant differences exist in the timing of rain initiation as well as the final rain-water contents among these schemes. The timing of rain initiation in the C&L scheme does respond to different aerosol types, being faster in the maritime scenario and slower in the continental scenario. However, when compared with the detailed model results the C&L scheme is less sensitive, with a delay or hastening of a few minutes. This is mainly due to the dependence of the autoconversion process on the dispersion of the cloud drop size, which is not resolvable in the C&L two-moment scheme. As for the final rain-water content, the C&L scheme follows the detailed model fairly closely, particularly in the maritime scenario. Note that the pattern of rain development in

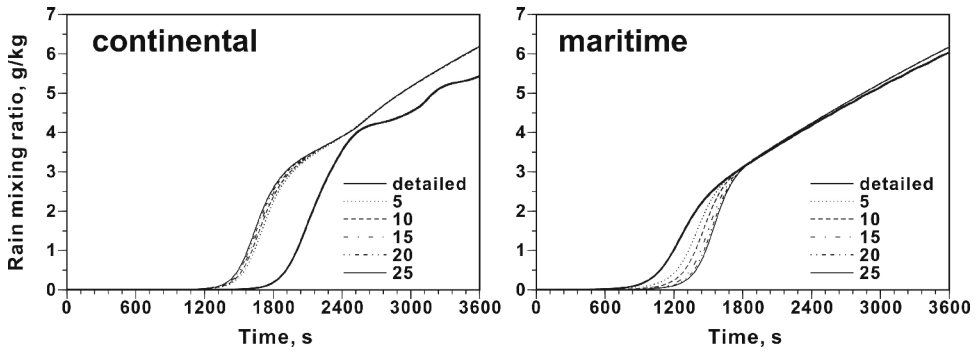

Figure 7. Rain-water evolution using the C&L scheme with different cut-off dry radius (thin curves labelled in μm) for rain embryos, comparing with that from the detailed model (thick curves). See text for details.

Kessler's scheme is closer to the maritime scenario of the detailed calculation, whereas the patterns in Lee's scheme are closer to those of the continental scenario.

In section 3(e) we mentioned that the timing of rain initiation may be improved by treating CCN with $r_{\mathrm{dry}} > 10$ μm as rain embryos, and putting them directly into the rain category when they are activated. Figure 7 show the sensitivity of rain development to the cut-off rain embryo size. For the maritime scenario a smaller cut-off size promotes faster rain development, and the result becomes closer to that of the detailed model for progressively smaller cut-off sizes. But this rain-embryo effect is less significant for the continental scenario due to the presence of fewer giant CCN. Note that for the case shown in Fig. 7 we select a 10 μm cut-off instead of the 5 μm that gives better results. This decision is made to avoid overstretching the size definition of raindrops and the use of conversion rate formulae that should not be extrapolated to too small sizes.

(*b*) *Supersaturation development*

In order to resolve accurately the cloud drop number concentration, the bulkwater scheme must be able to simulate the development of supersaturation with high precision. As shown in Fig. 8, the saturation ratio from the C&L scheme follows closely those from the detailed model, particularly during the activation stage. Kessler's scheme adopted the 'saturation adjustment' approach, which does not allow any supersaturation. As pointed out by Kogan and Martin (1994), large errors in the amounts of condensed water vapour and the latent heat released may result from the saturation adjustment schemes, particularly under conditions of low cloud drop number concentration. Although the scheme of Lee develops some degree of supersaturation, it does not produce a sharp decrease after the activation is completed as it should do. Again, supersaturation produced from neither Kessler's nor from Lee's scheme is sensitive to the aerosol types. Toward the later stage the saturation ratios from both the detailed and the C&L schemes begin to increase after a period of steadiness. This increase is due to the reduction of cloud drops by intensifying rain accretion, which causes a decrease in the overall condensation rate. In addition, the detailed parcel model shows pulsating features caused by the re-enabled activation events when the supersaturation exceeds the previous maximum (cf. Chen 1994a; Chen and Lamb 1999). In contrast, the C&L scheme shows much smoother changes.

Although the general trends are quite consistent, it is fair to ask why there are no pulsating features produced by the C&L scheme. One factor that is very different during

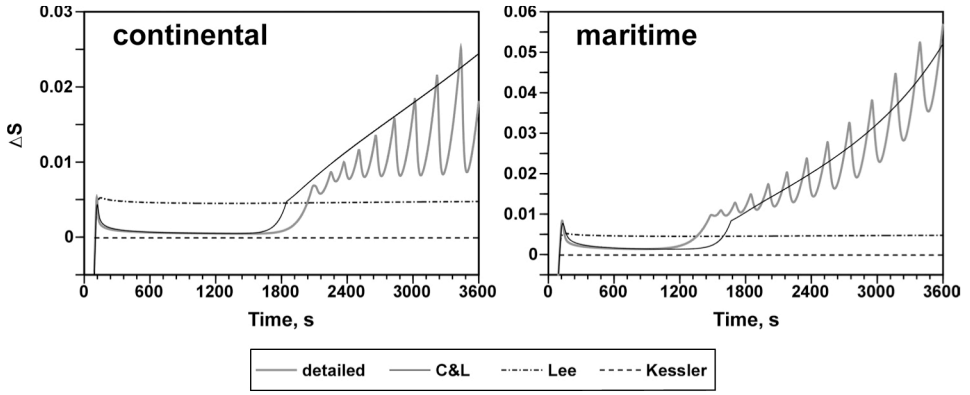

Figure 8. Same as in Fig. 6, but for the evolution of saturation ratio.

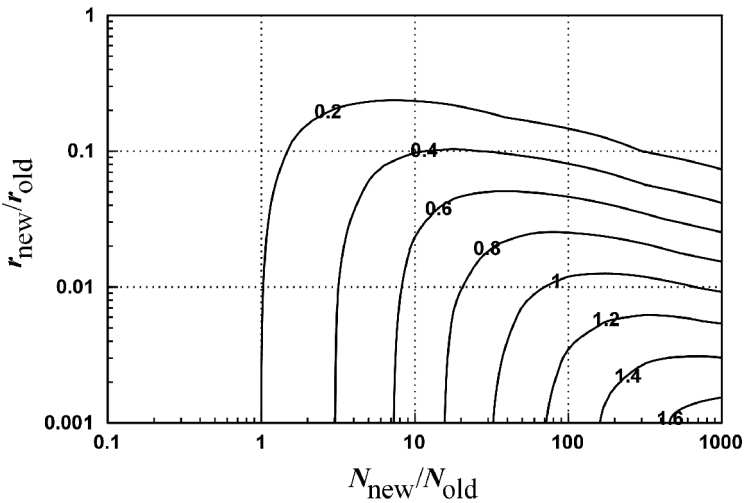

Figure 9. Ratio (in $\log_{10}$ scale) of the bulk and the actual condensation rates when two populations of monodispersed cloud drops coexist. The ordinate is the size ratio of the two populations, and the abscissa is the ratio of their number concentrations. See text for details.

the secondary activation compared with during the primary activation is the presence of existing droplets. As the new drops are activated, they have radii much smaller than those existing drops. Yet, such size dispersion cannot be resolved by the bulkwater scheme, so large errors may result in the overall condensation rate. Here we performed a simple calculation for two groups of monodispersed droplets to show this effect. Assume that the number concentration and radius of the existing drops are N_{old} and r_{old}, and those of the newly activated drops are N_{new} and r_{new}. According to Eq. (5), the actual condensation rate is proportional to $N_{old}r_{old} + N_{new}r_{new}$, but the bulk condensation rate is proportional to $(N_{old} + N_{new})r_C$, where $r_C = \{(N_{old}r_{old}^3 N_{new}r_{new}^3)/(N_{old} + N_{new})\}$. The ratios of these two condensation rates with the above definitions are plotted in Fig. 9. One can see that the overall condensation rate of the bulk representation is always greater than the actual value, and is greater when the newly activated drops are smaller or more numerous. For example, if the new drops are ten times smaller and

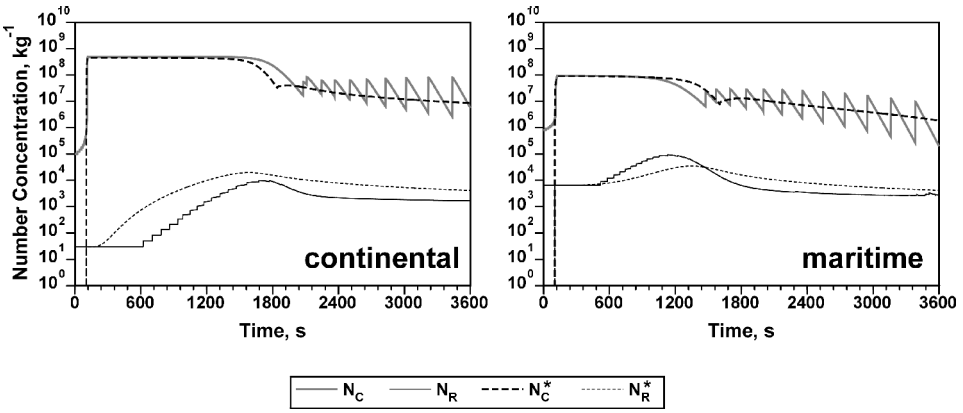

Figure 10. Comparison of the number concentration of cloud drops (upper curves) and raindrops (lower curves) calculated from the C&L scheme (dotted curves; N^* in the curve legend) and the detailed model (solid curves). See text for details.

ten times more numerous, the bulk condensation rate would be 2.5 ($10^{0.4}$) times that of the actual value. So the bulk scheme tends to artificially damp the development of supersaturation, thus diminishing the pulsation phenomenon. Ferrier (1994) as well as Carrió and Nicolini (2002) pointed out a similar effect, namely that an artificial change in the tail of the prescribed size distribution could result when new particles are added to the other end of the spectrum for bulkwater representation. Conceivably, mitigation may be obtained when a third moment is included in the bulkwater scheme to account for the size dispersion effect. Note that the pulsating feature produced by our parcel model might not be very common in multi-dimensional models, because of the more complicated dynamics and their allowing drop removal by sedimentation.

(*c*) *Number concentrations*

With accurate calculations of supersaturation, the C&L scheme is able to obtain cloud drop number concentrations very similar to those obtained from the detailed model. From Fig. 10 one can see that the C&L scheme can resolve the large difference in the initial (cloud-base) cloud drop number concentration between the continental and maritime aerosol scenarios. The pulsating feature in the later part of the detailed model is related to the variations in the supersaturation, as discussed previously. Although the bulk scheme did not produce the pulsating phenomenon, there is an indication of the re-enabled activation at around 1800 s simulation time, where the number concentration rebounded from a decreasing trend. Also shown in Fig. 10 are the raindrop number concentrations from these two schemes. Although the differences between them are more significant than those for cloud drops, the magnitudes and general trends are rather similar. Note that the number concentrations of cloud drops and raindrops are not zero before cloud formation in the detailed model, because there are haze droplets with sizes matching the cloud drop and raindrop size criteria.

In Fig. 10 the raindrop number concentration produced from our scheme first increases due to autoconversion. Then, as the larger cloud drops that more easily autoconvert to raindrops are gradually depleted, the raindrop number concentration starts to decrease due to raindrop self-collection. Eventually, raindrop growth by accretion or self-collection is balanced by collision break-up, so the raindrop number concentration as well as the mean volume radius (not shown), approach a steady state. Such a

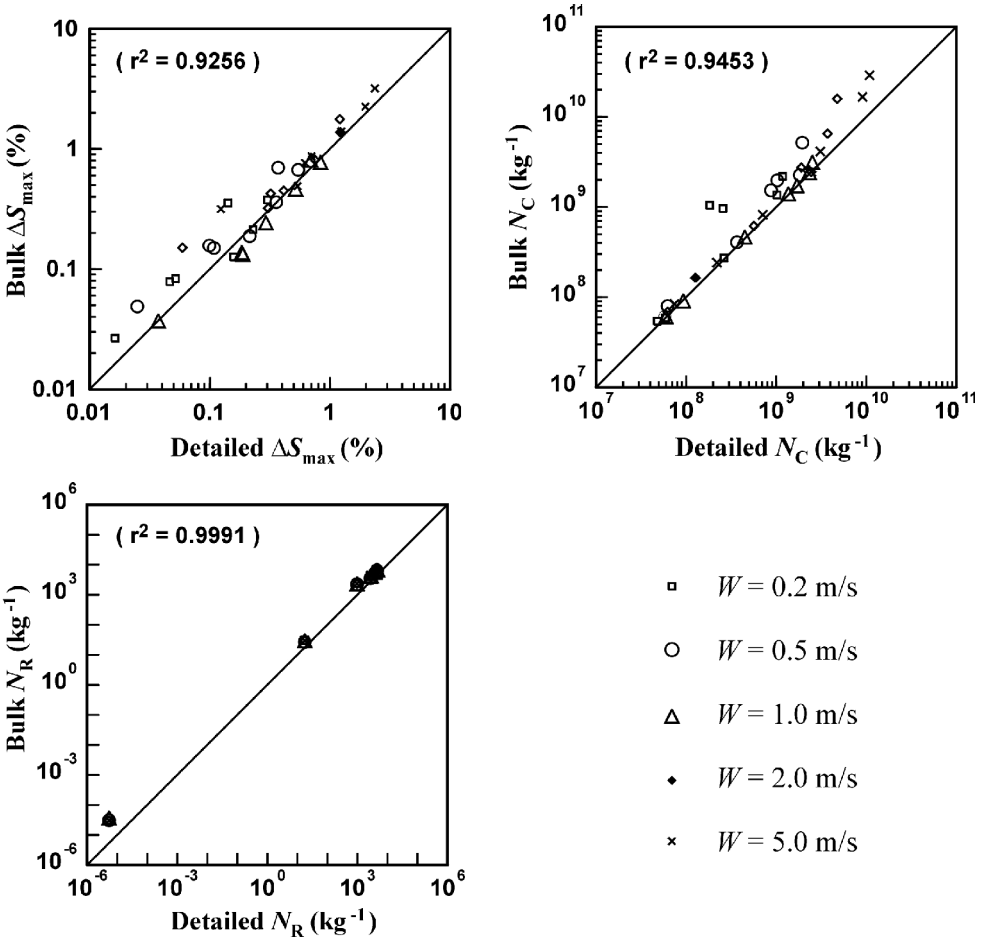

Figure 11. Comparison of the microphysical properties near the cloud base calculated with the detailed model and the C&L scheme: (a) maximum supersaturation, (b) cloud drop number concentration, and (c) raindrop number concentration. The symbols indicate different updraught speeds, and different points of the same symbol are for different aerosol types. See text for details.

steady-state result exists in all simulations we performed. This phenomenon is similar to the findings of Bringi *et al.* (2003)—that the median volume diameter measured with disdrometers tends to a constant value at high rain rates. It is also interesting to note that in our simulations the quasi-steady-state number concentration of raindrops, $N_{R,\infty}$, (around 2000 per kg of air) does not vary much ($\pm 10\%$) with the aerosol type, and varies moderately ($\pm 40\%$) with the cloud-base conditions (or the total condensable water). These results indicate that hydrodynamic interactions cause the raindrop size spectrum to evolve toward a steady state, at least in the bulk sense. The quasi-steady-state mean volume radius, $r_{R,\infty}$, gets larger with higher rain-water content, and the highest value from all simulations is 1.14 mm. One may convert the bulk properties (two moments) into a Marshall–Palmer distribution $n(r) = n_0 \exp(-\Lambda r)$, which has a slope Λ equal to $0.91/r_R$. As the actual mean volume radius from our scheme is always smaller than $r_{R,\infty}$, the Λ obtained from our scheme is always greater than about 0.8 mm^{-1}. These value ranges of r_R and Λ are consistent with the observations (Pruppacher and Klett 1997; Bringi *et al.* 2003).

TABLE 5. COMPARISON OF THE COMPUTATION EFFICIENCIES BETWEEN THE DETAILED MODEL AND THREE PARAMETRIZATION SCHEMES

	Detailed model	Kessler (1967)	Lee (1989)	C&L[1]
CPU time	848.1	0.2	0.2	0.2

[1]Chen and Lamb (1994, 1999)

(*d*) *General comparisons*

The results from other simulations are similar, so the details will not be elaborated here. Instead, we show some collective results. Squires (1958) and Twomey (1959) pointed out that $\Delta S_{\max}$ and N_C developed during the activation stage are controlled primarily by the aerosol type and updraught speed, so we focus on the sensitivity of the bulk scheme to these parameters. From the scatter plot in Fig. 11 one can see that $\Delta S_{\max}$ and N_C can vary by over two orders of magnitude with different controlling factors. Over these wide ranges of values, high correlations between the bulk and detailed results were achieved, with $r^2 = 0.926$ for $\Delta S_{\max}$ and $r^2 = 0.945$ for N_C. The less than ideal performances of the bulk scheme (against the detailed model) occur mostly with low updraught speeds or under polluted aerosol scenarios (i.e. the 'urban average' and 'background and local sources' of Whitby (1978)). Also shown in Fig. 11 are the number concentrations of raindrops, N_R, during the activation stage. More exactly, these are the rain embryos with $r_{dry} > 10$ μm. By our definition, N_R is determined by the aerosol types only and is not sensitive to the updraught speeds. So the bulk results correspond very well with the detailed results, with a high r^2 of 0.999. The minor discrepancies come mostly from the discrete nature of the aerosol bin sizing in the detailed model.

In general, the C&L scheme can reproduce the 'bulk properties' of the detailed model simulation with fairly high accuracy. Furthermore, it is very efficient computationally. Table 5 shows the computation time needed for one typical parcel-mode simulation. All these bulk schemes are over 4000 times faster than the detailed model. The C&L scheme is as fast as the other two bulk schemes even though it considers one more moment and thus has more rate equations to solve. However, with the additional moment, more time is needed in the calculation of particle advection in multi-dimensional models. Also, with more information on the spectral distribution of drops, it might be necessary to incorporate more sophisticated radiative transfer schemes in order to be consistent.

5. DISCUSSION

Most of the parametrization formulae in our scheme have r^2 values much higher than those in Lee (1989), as should be the case since we used one more moment than Lee. It is possible to obtain a falsely high r^2 by reducing the number of simulation scenarios (for example, the use of only one aerosol type). We have made sure that the more than 230 simulation scenarios we computed are sufficient to reach stable results. So, the r^2 values in Table 2 in effect represent the fundamental limitation of a two-moment scheme. At least a third moment is necessary to further improve the accuracy. This is particularly true for the two self-collections, autoconversion, break-up, and cloud drop deactivation processes that are dependent on the drop size dispersion.

The inclusion of the collision-break-up formulae (processes 7 and 8 in Table 1) is a significant improvement over most of the other bulkwater schemes, even though their r^2 values are not particularly high. Neglecting this process in a two-moment scheme allows the raindrops to grow to unrealistically large sizes, and may lead to biases in the

precipitation efficiency and in diagnosing radar reflectivity. Ziegler (1985) is among the few who considered collision-break-up in their bulkwater schemes, but he had to make simplifications in the fragment drop size distributions due to their very complicated forms, whereas our scheme considered all details of the formulations by Low and List (1982b) and the corrections in List *et al.* (1987).

Ferrier (1994), Carrió and Nicolini (2002) and a few others solved some of the growth equations numerically and stored the solutions in look-up tables. Such an approach is, in principle, similar to ours because they derive analytical solutions through numerical calculations. The main difference is that their numerical solutions were derived with prescribed size distributions, whereas ours were obtained through a detailed model calculation that let the size distribution evolve naturally. Our parametrization formulae are mostly simple forms and are easier to use than the look-up tables. Another advantage of formulae over look-up tables is that these formulae can be converted rather easily into characteristic frequencies or lifetimes, which may be useful in the scale analysis of each microphysical process.

Like many other parametrization schemes, our scheme cannot be applied to models of all scales. Wood *et al.* (2002) pointed out that large bias in the rates of autoconversion in stratiform boundary-layer clouds may occur due to the inhomogeneity of cloud water within a model grid box. Such a grid-resolution problem actually applies to essentially all microphysical conversion rates. For instance, the number of cloud drops activated at the cloud base is very sensitive to the saturation excess, which can be easily averaged out in a large grid box. Such subgrid biases in Eulerian models are also prone to occur in the vertical direction. As pointed out by Clark (1973, 1974), a low vertical resolution or large time step will cause an under prediction of the supersaturation and droplet concentration. One can see from Fig. 8 that $\Delta S_{\max}$ is normally determined within 30 to 50 seconds after the air reaches saturation (cloud base) for an updraught speed of 1 m s^{-1}. In this case the vertical grid resolution should be much finer than 50 m in order to resolve $\Delta S_{\max}$ and the cloud drop number concentration determined from it. As revealed by our simulations and others (e.g. Kogan 1991), this critical distance for activation is only of second order dependence on the updraught speed, and is typically about a few tens of metres. So, in general the vertical grid space near the cloud base should be around 10 m, but this criterion is most often not met. The biases resulting from the above grid-resolution problem will propagate to other processes listed in Table 1, because they are directly or indirectly related to the number concentration of cloud drops. Therefore, when our scheme is to be applied to models with large grid spaces, subgrid treatments such as those discussed in Wood *et al.* (2002) should be applied. Alternatively, a sub-module that contains only the equations of condensation rates and activation size from our scheme can be used in conjunction with a Lagrangian adiabatic calculation to determine $\Delta S_{\max}$ and initial N_C in the vicinity of the cloud base. Such a sub-module could be useful in dealing with subgrid or sub time step problems.

Our parametrization formulas are based on simulations of detailed microphysics in the parcel mode, which means we have neglected the effects of turbulence and entrainment. Many studies have pointed out the possible influence of turbulence and entrainment on the broadness of cloud drop size distribution. However, there are no conclusive results that may easily be applied to the parametrization of these influences. Part of the difficulty stems from the inability of regional- and cloud-scale models to resolve microscale structures that are associated with turbulence. Malinowski *et al.* (2000) showed that inhomogeneity of cloud properties may persist down to very small scales. Considering this small-scale inhomogeneity, artificial broadening of an observed cloud drop size distribution may result from a large sampling volume that is actually

an assemblage of air parcels with different evolution history. Numerical models have similar problems: everything in one grid box is well mixed no matter how large the grid. Treatment of turbulent mixing as a homogeneous process, as in most cloud models, may cause artificial modification of the drop spectrum. Thus, we took the parcel model approach to separate out turbulence effects. When a better theory is, or better data are, available, supplemental parametrization formulas can be derived and used in conjunction with the current scheme.

6. Conclusions

In this study we developed a new two-moment bulkwater parametrization scheme for warm-cloud microphysics. This C&L scheme can produce bulk properties of warm clouds similar to those from the detailed model of Chen and Lamb (1994), but with much higher computation efficiency. The microphysical processes considered in this C&L scheme are: the activation of aerosol particles into cloud drops, drop growth by vapour diffusion (condensation and evaporation), cloud drop self-collection, autoconversion of cloud drops into raindrops, cloud drop accretion by raindrops, raindrop self-collection, and collision break-up of raindrops.

The C&L scheme performs most excellently in simulating cloud properties during the activation stage of cloud formation. Both the maximum supersaturation and cloud drop number concentration obtained correlate very well with the detailed results over a wide range of ambient conditions. Therefore, this scheme is sensitive to the influence of different aerosol types on cloud processes. Less satisfactory accuracy was obtained for the parametrization of processes that depend heavily upon the broadness of the size distribution, such as autoconversion, self-collection, and break-up. Further improvement to these prognostic equations may be achieved by adding a third moment in the parametrization scheme. We provided several diagnostic equations for cloud microphysical properties, including the group fall speeds, number and mass sedimentation fluxes, radar reflectivity factor, and the effective radii of cloud drops and raindrops. Most of these prognostic and diagnostic equations were formulated in simple forms but expressive in their physics, as demonstrated by a few examples with detailed discussions.

In principle, our approach can be used in deriving parametrizations for other atmospheric physical processes. The next feasible choice is the investigation of ice-phase cloud processes. However, ice particles have complicated physical structures that are important to essentially all microphysical processes; in our opinion, at least two more parameters (moments) are needed to resolve the higher degrees of freedom, i.e. shape and density. The C&L model we used can also describe most of the important ice-phase microphysical processes, with details including the evolution of shapes and densities of ice particles. However, for a four-moment bulk scheme the collision-rate equations could contain up to eight bulk parameters, which will not be easy to formulate. Our next task is to solve the complicated procedure of parametrization on the ice microphysics by Chen and Lamb modelling, as well as implementing the parametrization scheme in regional or cloud-resolving models. Further study will also include the parametrization of aerosol microphysics and their interaction with clouds.

Acknowledgements

This research was supported by the National Science Council of the Republic of China under Grant NSC 89-2111-M-002-014 and NSC 90-2111-M-002-026. The comments and suggestions from T.-M. Fu, C.-T. Cheng and the anonymous reviewers are greatly appreciated.

APPENDIX

List of symbols, terms and units used

$\mathrm{dB}Z$	logarithmic radar reflectivity factor, $\equiv 10 \log_{10} Z$
D_v	diffusion coefficient of water vapour, $\mathrm{m}^2\ \mathrm{s}^{-1}$
e_sw	saturation vapour pressure, Pa
E	collection efficiency
E_coal	coalescence efficiency
FN	sedimentation flux of number concentration, particle $\mathrm{s}^{-1}\mathrm{m}^2$
FQ	sedimentation flux of mixing ratio, kg $\mathrm{s}^{-1}\mathrm{m}^2$
k_a	thermal conductivity of air, W $\mathrm{m}^{-1}\mathrm{K}^{-1}$
K	collision kernel
L_v	latent heat of vaporization, J kg^{-1}
m	drop mass
n	number density function
N	number concentration, particle kg^{-1} of air
$\dot{N}$	number concentration production rate, particle kg^{-1} of air s^{-1}
P	air pressure, Pa
Q	mixing ratio, kg kg^{-1}
$\dot{Q}$	mixing ratio production rate, kg $\mathrm{kg}^{-1}\mathrm{s}^{-1}$
r	correlation coefficient
r_d	drop radius
$\overline{r}_\mathrm{d}$	mean number radius (defined in Eq. 19), m
r_0	equilibrium radius of drops at $S = 1$, m
r_act	cloud drop radius at the time of activation, m
r_C	mean volume radius of cloud drops (defined in Eq. 7), m
r_dry	dry (residual after evaporation) radius of drops, m
r_e	effective radius (defined in Eq. 13), m
r_L	radius of the larger drop of colliding drop pair, m
r_R	mean volume radius of raindrops, m
r_S	radius of the smaller drop of colliding drop pair, m
R_v	gas constant of water vapour, J $\mathrm{kg}^{-1}\mathrm{K}^{-1}$
S	saturation ratio
S_eq	equilibrium saturation ratio of drops
ΔS	supersaturation
t	time, s
T	air temperature, K
U	terminal velocity, m s^{-1}
W	updraught speed, ms^{-1}
Z	radar reflectivity factor, $\mathrm{mm}^6\mathrm{m}^{-3}$
β_C	$\equiv r_\mathrm{e} / r_\mathrm{C}$
ε	dispersion of the drop size spectrum (defined in Eq. 16)
γ	skewness of the drop size spectrum (defined in Eq. 17)
Λ	slope of the Marshall–Palmer distribution
ρ_a	air density, kg m^{-3}
ρ_w	water density, kg m^{-3}
σ	standard deviation of the drop size spectrum (defined in Eq. 18), m

Subscripts:

a	air
d	drop/droplet
C	cloud drops
R	raindrops
v	water vapour
w	liquid water

REFERENCES

Albrecht, B. A. 1989 Aerosols, cloud microphysics, and fractional cloudiness. *Science*, **262,** 226–229

Alkezweeny, A. J., Burrows, D. A. and Grainger, C. A. 1993 Measurement of cloud-droplet size distributions in polluted and unpolluted stratiform clouds. *J. Appl. Meteorol.*, **32,** 106–115

Beard, K. V. and Ochs H. T. III. 1984 Collection and coalescence efficiencies for accretion. *J. Geophys. Res.*, **89,** 7165–7169

Berry, E. X. and Reinhardt, R. L. 1973 *Modeling of condensation and collection within clouds*. Physical Sciences Publication No. 16, University of Nevada, Reno, USA

Blyth, A. M. and Latham, J. 1991 A climatological parameterization of cumulus clouds. *J. Atmos. Sci.*, **48,** 2367–2371

Böhm, J. P. 1992a A general hydrodynamic theory for mixed-phase microphysics. Part I: Drag and fall speed of hydrometeors. *Atmos. Res.*, **27,** 253–274

1992b A general hydrodynamic theory for mixed-phase microphysics. Part II: Collision kernels for coalescense. *Atmos. Res.*, **27,** 275–290

Bringi, V. N., Chandrasekar, V., Hubbert, J., Gorgucci, E., Randeu, W. L. and Schoenhuber, M. 2003 Raindrop size distribution in different climatic regimes from disdrometer and dual-polarized radar analysis. *J. Atmos. Sci.*, **60,** 354–365

Carrió, G. G. and Nicolini, M. 2002 An alternative procedure to evaluate number concentration rates in two-moment bulk microphysical schemes. *Atmos. Res.*, **65,** 93–108

Chen, J.-P. 1994a Predictions of saturation ratio for cloud microphysical methods. *J. Atmos. Sci.*, **51,** 1332–1338

1994b Theory of deliquescence and modified Köhler curves. *J. Atmos. Sci.*, **51,** 3505–3516

Chen, J.-P. and Lamb, D. 1994 Simulation of cloud microphysical and chemical processes using a multicomponent framework. Part I: Description of the microphysical model. *J. Atmos. Sci.*, **51,** 2613–2630

1999 Simulation of cloud microphysical and chemical processes using a multicomponent framework. Part II: Microphysical evolution of a wintertime orographic cloud. *J. Atmos. Sci.*, **56,** 2293–2312

Chen, J.-P., McFarquhar, G. M., Heymsfield, A. J. and Ramanathan, V. 1997 A modeling and observational study of the detailed microphysical structure of tropical cirrus anvils. *J. Geophys. Res.*, **102,** 6637–6653

Clark, T. L. 1973 Numerical modeling of the dynamics and microphysics of warm cumulus convection. *J. Atmos. Sci.*, **30,** 857–878

1974 A study in cloud phase parameterization using the gamma distribution. *J. Atmos. Sci.*, **31,** 142–155

Clark, T. L. and Hall, W. D. 1983 A cloud physical parameterization method using movable basis functions: Stochastic coalescence parcel calculations. *J. Atmos. Sci.*, **40,** 1709–1728

Del Genio, A. D., Yao, M.-S., Kovari, W. and Lo, L. W. 1996 A prognostic cloud water parameterization for global climate models. *J. Climate*, **9,** 270–304

Doviak, R. J. and Zrnic, D. S. 1984 *Doppler radar and weather observations*. Academic Press, San Diego, USA

Feingold, G., Stevens, B., Cotton, W. R. and Frisch, A. S. 1996 On the relationship between drop in-cloud residence time and drizzle production in numerically simulated startocumulus clouds. *J. Atmos. Sci.*, **53,** 1108–1122

Ferrier, B. S. 1994 A double-moment multi-phase four-class bulk ice scheme. Part I: Description. *J. Atmos. Sci.*, **51,** 249–280

Fouquart, Y., Buriez, J. C., Herman, M. and Kandel, R. S. 1990 The influence of clouds on radiation: A climate-modeling perspective. *Rev. Geophys.*, **28,** 145–166

Fowler, L., Randall, D. A. and Rutledge, S. A. 1996 Liquid and ice cloud microphysics in the CSU general circulation model. Part II: Impact on cloudiness, the earth's radiation budget, and the general circulation of the atmosphere. *J. Climate*, **9,** 530–560

Giorgi, F., Huang, Y., Nishizswa, K. and Fu, C. 1999 A seasonal cycle simulation over eastern Asia and its sensitivity to radiative transfer and surface processes. *J. Geophys. Res.*, **104,** 6403–6423

Gong, W. and Wang, W.-C. 2000 A regional model simulation of the 1991 severe precipitation events over the Yangtze–Huai river valley. Part II: Model bias. *J. Climate*, **13,** 93–108

Green, A. W. 1975 An approximation for the shapes of large raindrops. *J. Appl. Meteorol.*, **14,** 1578–1583

Hegg, D. A., Radke, L. F. and Hobbs, P. V. 1991 Measurements of Aitken nuclei and cloud condensation nuclei in the marine atmosphere and their relation to the DMS-cloud-climate hypothesis. *J. Geophys. Res.*, **96,** 18727–18733

Hu, Z., Bruinjes, R. T. and Betterton, E. A. 1998 Sensitivity of cloud droplet growth to collision and coalescence efficiencies in a parcel model. *J. Atmos. Sci.*, **55,** 2502–2515

IPCC 2001 *Intergovernmental panel on climate change, Climate change 2001: The scientific basis*. Eds. J. T. Houghton, Y. Ding, D. J. Griggs, M. Noguer, P. J. van der Linden and D. Xiaosu. Cambridge University Press, Cambridge, UK

Jaenicke, R. 1993 Tropospheric aerosols. Pp. 1–31 in: *Aerosol–cloud–climate interactions*. Ed. P. V. Hobbs. Academic Press, New York, USA

Joss, J. and Gori, E. G. 1978 Shapes of raindrop size distribution. *J. Appl. Meteorol.*, **17,** 1054–1061

Kessler, E. 1967 'On the continuity of water substance'. ESSA Technical Memorandum IERTM-NSSL 33. National Severe Storms Laboratory, Norman, USA

1969 *On the distribution and continuity of water substance in atmospheric circulation*. Meteorological Mongraph No. 10, American Meteorological Society, Boston, USA

Khairoutdinov, M. and Kogan, Y. L. 2000 A new cloud physics parameterization in a large-eddy simulation model of marine stratocumulus. *Mon. Weather Rev.*, **128,** 229–243

Kiehi, J. T. 1994 Sensitivity of a GCM climate simulation to differences in continental versus maritime cloud drop size. *J. Geophys. Res.*, **99,** 23107–23115

Kogan, Y. L. 1991 The simulation of a convective cloud in a 3-D model with explicit microphysics. Part I: Model description and sensitivity experiments. *J. Atmos. Sci.*, **48,** 1160–1189

Kogan, Y. L. and Martin, W. J. 1994 Parameterization of bulk condensation in numerical cloud models. *J. Atmos. Sci.*, **51,** 1728–1739

Kreidenweis, S. M., Walcek, C. J., Feingold, G., Gong, W., Jacobson, M. Z., Kim, C.-H., Liu, X., Penner, J. E., Nenes, A. and Seinfeld, J. H. 2003 Modification of aerosol size distribution due to aqueous-phase SO_2 oxidation in clouds: Comparisons of several models. *J. Geophys. Res.*, **108,** doi: 10.1029/2002JD002697

Lee, I. Y. 1989 Evaluation of cloud microphysics parameterizations for mesoscale simulations. *Atmos. Res.*, **24,** 209–220

1992 Comparison of cloud microphysics parameterizations for simulations of mesoscale clouds and precipitation. *Atmos. Environ.*, **26A,** 2699–2712

Lin, Y.-L., Farley, R. D. and Orville, H. D. 1983 Bulk parameterization of the snow field in a cloud model. *J. Clim. Appl. Meteorol.*, **22,** 1065–1092

List, R., Donaldson, N. R. and Stewart, R. E. 1987 Temporal evolution of drop spectra to collisional equilibrium in steady and pulsating rain. *J. Atmos. Sci.*, **44,** 362–372

Liu, Y. 1993 Statistical theory of the Marshall–Palmer distribution of raindrops. *Atmos. Environ.*, **27A,** 15–19

Liu, Y. and Daum, P. H. 2002 Indirect warming effect from dispersion forcing. *Nature*, **419,** 580–581

Lohmann, U., Feichter, J., Chung, C. C. and Penner, J. E. 1999 Prediction of the number of cloud droplets in the ECHAM GCM. *J. Geophys. Res.*, **104,** 9169–9198

Low, T. B. and List, R. 1982a Collision, coalescence and breakup of raindrops. Part I: Experimentally established coalescence efficiencies and fragment size distribution in breakup. *J. Atmos. Sci.*, **39,** 1591–1606

1982b Collision, coalescence and breakup of raindrops. Part II: Parameterization of fragment size distributions. *J. Atmos. Sci.*, **39,** 1607–1618

Malinowski, S. P., Haman, K. E., Andrejczuk, M., Banat, P. and Jaczewski, A. 2000 'Small-scale properties of clouds: Summary of recent results from aircraft measurements, laboratory experiments and numerical modeling'. Pp. 109–112 in Proceedings of the international conference on clouds and precipitation, Reno. American Meteorological Society, Boston, USA

Manton, M. J. and Cotton, W. R. 1977 Formulation of approximate equations for modeling moist deep convection on the mesocale. Atmospheric Science Paper No. 266, Department of Atmospheric Sciences, Colorado State University, USA

Marshall, J. S. and Palmer, W. 1948 The distribution of raindrops with size. *J. Meteorol.*, **5,** 165–166

Martin, G. M., Johnson, D. W. and Spice, A. 1994 The measurement and parameterization of effective radius of droplets in warm stratocumulus clouds. *J. Atmos. Sci.*, **51,** 1823–1842

Moeng, C.-H. and Curry, J. 1990 'The sensitivity of large eddy simulations of a stratus topped boundary layer to cloud microphysics'. Pp. 115–121 in Proceedings of the conference of cloud physics, San Francisco. American Meteorological Society, Boston, USA

Mölders, N., Hass, H., Jakobs, H. J., Laube, M. and Ebel, A. 1994 Some effects of different cloud parameterizations in a mesoscale model and a chemistry transport model. *J. Appl. Meteorol.*, **33,** 527–545

Pontikis, C. A. and Hicks, E. M. 1992 Contribution to the cloud droplet effective radius parameterization. *Geophys. Res. Lett.*, **19,** 2227–2230

Pruppacher, H. R. and Klett, J. D. 1997 *Microphysics of clouds and precipitation*. Kluwer Academic Publishers, Dordrecht, the Netherlands

Qian, J. and Law, C. K. 1997 Regimes of coalescence and separation in droplet collision. *J. Fluid Mech.*, **331,** 59–80

Rosenfeld, D. 2000 Suppression of rain and snow by urban and industrial air pollution. *Science*, **287,** 1793–1796

Silverman, B. A. and Glass, M. 1973 A numerical simulation of warm cumulus clouds: Part I. Parameterized vs non-parameterized microphysics. *J. Atmos. Sci.*, **30,** 1620–1637

Squires, P. 1958 The microstructure and colloidal stability of warm clouds. *Tellus*, **10,** 262–271

Srivastava, R. C. 1978 Parameterization of raindrop size distributions. *J. Atmos. Sci.*, **35,** 108–117

Stevens, G. L. 1978 Radiation profiles in extended water clouds. II: Parameterization schemes. *J. Atmos. Sci.*, **35,** 2123–2132

Stevens, B., Cotton, W. R., Feingold, G. and Moeng, C.-H. 1998 Large-eddy simulations of strongly precipitating, shallow, stratocumulus-topped boundary layers. *J. Atmos. Sci.*, **55,** 3616–3638

Tripoli, G. J. and Cotton, W. R. 1980 A numerical investigation of several factors contributing to the observed variable intensity of deep convection over south Florida. *J. Appl. Meteorol.*, **19,** 1037–1063

Twomey, S. 1959 The nuclei of natural cloud formation, Part II: The supersaturation in natural clouds and the variation of cloud droplet concentration. *Geofys. Pura e Appl.*, **43,** 243–249

1974 Pollution and the plantary albedo. *Atmos. Environ.*, **8,** 1251–1256

Valdez, M. P. and Young, K. 1985 Number fluxes in equilibrium raindrop populations: A Markov chain analysis. *J. Atmos. Sci.*, **42,** 1024–1036

Whitby, K. T. 1978 The physical characteristics of sulfur aerosols. *Atmos. Environ.*, **12,** 135–159

Willis, P. T. 1984 Functional fits to some observed drop size distributions and parameterization of rain. *J. Atmos. Sci.*, **41,** 1648–1661

Wisner, C., Orville, H. D. and Myers, C. 1972 A numerical model of a hail-bearing cloud. *J. Atmos. Sci.*, **29,** 1160–1181

Wood, R., Field, P. R. and Cotton, W. R. 2002 Autoconversion rate bias in stratiform boundary layer cloud parameterizations. *Atmos. Res.*, **65,** 109–128

Zawadzki, I., Monteiro, E. and Fabry, F. 1994 The development of drop size distributions in light rain. *J. Atmos. Sci.*, **51,** 1100–1113

Ziegler, C. L. 1985 Retrieval of thermal and microphysical variables in observed convective storms. Part 1: Model development and preliminary testing. *J. Atmos. Sci.*, **42,** 1487–1509